

STABILIZED CVD AMORPHOUS SILICON FOR HIGH TEMPERATURE PHOTOTHERMAL SOLAR ENERGY CONVERSION*

D. C. BOOTH, D. D. ALLRED and B. O. SERAPHIN
Optical Sciences Center, University of Arizona, Tucson, AZ 85721, USA

Received 5 July 1979

By pyrolytic decomposition of silane in the presence of dopant gases, a set of amorphous silicon films was prepared that contains various concentrations of carbon, nitrogen, boron or germanium. The effect of these dopants on the crystallization process and the optical properties is investigated. Films containing about 18 at% carbon show the properties most favorable for solar absorbers. The crystallization is retarded to temperatures near 1000°C, and the solar absorptance is greater than that of non-intentionally doped CVD amorphous silicon. From the experimentally determined activation energy of crystallization, the structural lifetime for such absorber films is extrapolated to be in excess of several decades for continuous operation at 700°C. For identical thicknesses of absorber layers, spectrally selective stacks of stabilized amorphous silicon deposited on top of a molybdenum reflector have higher solar absorptance than stacks composed of polycrystalline silicon on a silver reflector, amorphous silicon on molybdenum having been tested at temperatures in excess of 500°C.

1. Introduction

Efficient conversion of solar radiation into high-temperature heat requires surfaces capable of large absorption over the solar emission range, which at the same time reduce the thermal emission losses in the infrared [1-3]. Short of finding one single material of sufficient spectral selectivity, a standard approach to the problem employs the tandem action of a semiconductor absorber deposited on top of a reflector [4]. Strong interband transitions in the semiconductor provide the solar absorptance. At photon energies smaller than its energy gap, the absorber turns transparent, permitting the underlying reflector to suppress the emittance in the thermal infrared [5].

The optical response of most spectrally selective surfaces can be reduced to such a semiconductor-on-reflector tandem [6]. Silicon has long been a favored candidate for the absorber material, since its absorption edge falls approximately between the solar emission band and the spectral range of the thermal re-emission [7]. Using the technological benefits of chemical vapor deposition (CVD), a spectrally selective surface based on a silicon absorber was developed that permitted photothermal conversion at a temperature of 500°C [8, 9].

*Work supported by the U.S. Department of Energy, Office of Basic Energy Sciences, under Contract ER-78-S-02-4899.

In this initial work the silicon absorber was prepared at temperatures in excess of 700°C, where the pyrolytic decomposition of silane is rapid, resulting in the deposition of polycrystalline silicon. The absorption edge of this polycrystalline material is shallow and located spectrally in such a manner that too many infrared solar photons are permitted to pass through unabsorbed [10]. It was long known that the absorption profile of amorphous silicon is superior to that of polycrystalline silicon with respect to steepness and spectral position, thereby providing larger solar absorptance [11–13]. Sputtered or evaporated amorphous silicon, however, was known to crystallize rapidly at 550°C [14]. The resultant converter surfaces would have too short a lifetime at operating temperatures necessary for sufficient Carnot efficiency. It consequently appeared that the silicon phase having superior optical performance had to be ruled out on the basis of insufficient temperature stability.

Chemical vapor deposition of amorphous silicon improved the situation, however. Incomplete decomposition of the silane molecule led to the incorporation of hydrogen in the growing film. The resultant material, having a hydrogen content of 1 at% or less, did not crystallize as rapidly as its sputtered or evaporated counterparts. Detailed studies showed that crystallization in amorphous silicon is a gradual process that depends on length and temperature of anneal, and proceeds exponentially at higher temperatures. With this in mind, a “crystallization temperature” of 680°C for CVD amorphous silicon can be assigned for comparison with the crystallization temperature of 550°C previously observed for sputtered or evaporated amorphous silicon films [15].

In spite of this improvement, the thermally activated crystallization kinetics of CVD amorphous silicon implied that a converter operated at 500°C would have an insufficient lifetime. The coincidence of increased resistance to crystallization with the presence of hydrogen in amorphous silicon suggested that intentional dopants could retard even further the crystallization of CVD amorphous silicon. One constraint in this search was the requirement that the favorable optical properties of non-intentionally doped material be conserved in the stabilized phase. This paper describes a study of the effects of chosen dopants – C, N, B, and Ge – on the crystallization behavior of CVD amorphous silicon. Carbon was given the greatest attention because the solar absorptance of the alloyed material exceeded even that of the non-intentionally doped material. In addition, in alloys of silicon with carbon or nitrogen, the crystallization is retarded to a point where lifetimes of decades at temperatures in excess of 700°C can be predicted.

2. Experimental procedure

2.1. Sample preparation

Samples were prepared by the pyrolytic decomposition of silane and dopant gases onto fused quartz substrates in a horizontal, radiation heated, atmospheric pressure reactor. A helium carrier gas flow rate of typically 4 l/min was used. Two sources of silane were used, one nominally pure, and the other diluted to 11.5% in helium. Dopant

gases used were NH_3 (100%), C_2H_2 , B_2H_6 and GeH_4 , the latter three diluted to 1% in helium. Of the total gas flow, silane constituted typically 0.5% and the dopant gases typically 0.05%. Deposition temperatures ranged from 550 to 750°C and were determined with an accuracy of $\pm 5^\circ\text{C}$. Deposition rates ranged from 350 to 1300 Å/min, depending on temperature and dopant gas concentration. Most films were $(1.0 \pm 0.20) \mu\text{m}$ in thickness, and the film growth was monitored in situ using an infrared interference technique [16]. Fifty carbon-doped, 12 nitrogen-doped, 8 boron-doped, and 16 germanium-doped amorphous silicon samples were prepared. In addition, 20 undoped amorphous silicon samples were prepared as control samples.

2.2. Thickness measurements

The thickness of the films was measured with a Mirau two-beam interference objective on a Leitz microscope, after etching a step in the doped silicon film. The etchant solution consisted of 10% HF and 90% HNO_3 by volume, although for samples heavily doped with carbon or nitrogen, up to 50% HF and 50% HNO_3 was used. The interferograms were recorded in both white and monochromatic (5460 Å) light, enlarged and analyzed. Using this method, absolute thicknesses were measured with an accuracy of $\pm 200 \text{ Å}$. For most films studied, this resulted in a relative accuracy of the thickness determination of $\pm 2\%$.

In order to verify these measurements, selected samples were measured using a Dektak profilometer. These measurements were accurate to approximately $\pm 100 \text{ Å}$, and showed our calculated thicknesses to be within the range of accuracy of $\pm 200 \text{ Å}$ stated above.

2.3. Optical measurements

Optical properties of the silicon films were determined from transmittance and reflectance measurements made on two Perkin – Elmer spectrophotometers, model 137 ($2.5 \mu\text{m} \leq \lambda \leq 15.0 \mu\text{m}$) and model 450 ($0.35 \mu\text{m} \leq \lambda \leq 2.7 \mu\text{m}$). Aluminum references were used for reflectance measurements, and a holmium glass reference was used as a wavelength standard. Optical traces were partially reduced with the aid of a computer controlled digitizer having an absolute accuracy of 0.005" (0.13-mm) and a relative wavelength accuracy of better than 0.001 μm .

The refractive index of each film was calculated from the spectral positions of the minima of interference fringes of reflected light or the maxima of interference fringes of transmitted light. The refractive index calculations were made in the wavelength region where the absorption coefficient α was less than $5 \times 10^4 \text{ cm}^{-1}$.

The absorption coefficient was calculated from the transmittance, T , according to [17]:

$$T = \frac{(1 - R_1)(1 - R_2)(1 - R_3)e^{-\alpha d}}{1 - R_2R_3 + (2R_1R_2R_3 - R_1R_2 - R_1R_3)e^{-2\alpha d}}, \quad (1)$$

where R_1 , R_2 and R_3 are the reflectances of the air–film, film–substrate, and substrate–air interfaces, respectively, and d is the film thickness. In the near infrared, the inter-

ference fringes were averaged by using only the values of the transmittance at wavelengths that correspond to the mean values of the wavenumbers of adjacent minima and maxima. Values of α are reported only for $\alpha > 10^3 \text{ cm}^{-1}$, due to the large errors at lower values resulting from surface roughness and scattering, surface oxide and uncertainties in refractive index and thickness. For more specific details on the determinations of refractive index and absorption coefficient, the reader is referred to the work of Janai and his coworkers [15].

2.4. Annealing procedure

Samples were annealed in the center zone of a tube furnace with a flowing N_2/H_2 atmosphere of $70 \text{ cm}^3/\text{min}$, the H_2 content being 8.5%. Hydrogen was necessary to prevent the rapid oxidation of the silicon samples which were by necessity annealed at temperatures in excess of 900°C . Groups of samples were annealed at a constant temperature for varying amounts of time. The annealing temperature of a sample in the center of the set of samples was monitored to $\pm 1^\circ\text{C}$, the accuracy for the remaining samples within an anneal being $\pm 5^\circ\text{C}$. Before and after each anneal, the optical transmittance and reflectance, and the X-ray diffraction pattern were measured. After insertion into the annealing furnace, the samples reached annealing temperature within three minutes. No overshoot in temperature was observed, and the annealing times started when the samples were inserted into the furnace.

3. Characterization of the samples

3.1. Structural characterization

X-ray diffraction measurements displayed by a General Electric model XRD-5 X-ray diffractometer insured that the as-deposited material was amorphous. They also monitored the progress of crystallization during high temperature anneals. The absence of the $\text{Si}\{111\}$ diffraction peak (Cu K_α X-rays at $2\theta = 28.4^\circ$) was regarded as evidence of an amorphous structure. On selected samples, scans were made over a wide range of angles up to 90° to confirm that no crystalline phases were formed.

Using transmission electron microscopy (TEM), we studied the microscopic changes which occur in carbon-doped amorphous silicon (18 at% C) during high temperature anneal [18]. The samples were deposited onto carbon-coated copper grids previously passivated with 250 \AA of CVD Si_3N_4 to avoid substrate-film interaction.

3.2. Compositional analysis

Quantitative elemental analysis was performed by electron microprobe analysis, backscattering spectroscopy and secondary ion mass spectroscopy (SIMS). Of the three, the electron microprobe (an Applied Research Laboratory Scanning Electron Microprobe Quantometer) was most consistently used. The system is minicomputer

controlled and includes data analysis programs to correct for matrix effects. Charge buildup was partially avoided by overcoating the sample with a conducting film or by depositing the amorphous silicon film on a conducting surface such as a thin molybdenum film deposited on fused quartz.

The B, C, N and Ge content of our films was quantitatively determined by: 1) lowering the energy of the excitation electron beam to 5 keV so that the X-ray yield from the dopants was enhanced compared to the silicon matrix, 2) increasing the spot size to avoid surface contamination, and 3) by using calibration standards. CVD Si_3N_4 was used as the nitrogen calibration standard while a carbon-doped amorphous silicon film whose concentration had been determined by backscattering was used for the carbon calibration standard. A nominally pure CVD germanium film was used as the calibration standard for Ge doped samples.

Table 1 summarizes the composition of various of the doped amorphous silicon films. Certain deposition parameters are included for comparison purposes. For a few samples, the composition of the films was microprobed at several representative points to determine compositional variation. Within 10% of the measured value, no compositional variations were observed over the $5 \times 5 \text{ cm}^2$ deposition area. Thickness variations across the same area were typically 5%, contrasted with the uncertainty on the order of 2% in the thickness determination.

Samples prepared on quartz substrates are very smooth to the eye, except for films containing more than 22 at% C. All other dopants – N, B and Ge – produce very smooth films at all concentrations studied. As the carbon concentration increases beyond 22 at%, and for some high nitrogen concentrations as well, films crack upon cooling from deposition temperatures.

Table 1
Representative compositions and CVD process parameters for doped amorphous silicon

Dopant	Composition (at%) [†]	Substrate temperature	Dopant gas	Molar ratio of dopant gas to silane*	Deposition rate ($\text{\AA}/\text{min}$)
C	3.4	630	C_2H_2	0.004	1050
C	11.5	630	C_2H_2	0.021	700
C	18.0	630	C_2H_2	0.060	840
C	27.0	630	C_2H_2	0.096	520
C	35.0	630	C_2H_2	0.11	520
C	15.5	630	C_2H_2	0.060	1020
C	13.0	700	C_2H_2	0.060	1330
C	23.0	750	C_2H_2	0.060	640
N	17	575	NH_3	0.63	640
N	34	630	NH_3	0.56	740
B	<0.5	600	B_2H_6	0.006	1040
B	0.7	600	B_2H_6	0.056	680
Ge	1.9	630	GeH_4	0.23	680
Ge	11	600	GeH_4	1.12	820

*Silane at 0.02 l/min added to helium carrier to give a total flow rate of approximately 4.4 l/min.

[†]Precision of compositional determinations was 10% for Ge and C, 20% for N and 50% for B.

All as-deposited doped silicon films are amorphous, except for samples having a high boron concentration. The average diameter of coherently scattering regions as determined from the angular width of the Si{111} peak is 20 Å, as is the case for the non-intentionally doped material.

3.3. Electron spin resonance

The electron spin resonance of selected carbon-doped and non-intentionally doped amorphous silicon samples was measured by Gaczi [19] of the James Franck Institute, University of Chicago, Illinois, USA, and compared to similar measurements on glow discharge amorphous silicon.

3.4. Hydrogen content of non-intentionally doped amorphous silicon

The optical and structural properties of what we now term non-intentionally doped amorphous silicon have previously been reported by Janai and his colleagues [15]. The hydrogen content of this material as determined by secondary ion mass spectroscopy (SIMS) by Magee [20] of the RCA Labs was briefly mentioned in this paper. Samples were prepared on electrically conductive glass to insure electrical neutrality during analysis. We now show in fig. 1 the hydrogen content of non-intentionally doped amorphous silicon as a function of substrate temperature. Pyrolytically deposited amorphous silicon contains much less hydrogen than material made by glow-discharge at a much lower substrate temperature, which typically contains 2–30 at% hydrogen in as-deposited films [21].

4. Experimental results and discussion

4.1. Effects of doping on crystallization

Janai et al. [15] reported that CVD amorphous silicon, unlike all other films deposited at temperatures much below 600°C, is anneal-stable below the onset of crystallization. Increasing the temperature and/or the time of an anneal induces progressive crystallization, as indicated by the appearance and subsequent growth of the silicon {111} peak. The absorption edge moves to shorter wavelengths after an initial red shift, and the refractive index decreases. Our results on non-intentionally doped amorphous silicon films confirm the observations of Janai and coworkers.

In contrast, CVD amorphous silicon films doped with carbon, nitrogen, boron or germanium apparently differ in the way the crystallization proceeds, as judged from the response of the X-ray spectra, as well as from the optical properties, to annealing at various temperatures and for various lengths of time. In the non-intentionally doped, rather pure material, the crystallization proceeds throughout the entire volume, starting from random crystallization centers embedded in the amorphous matrix. Since the hydrogen content is small in a sample about to crystallize, the impurity concentrations inside and outside the growing nucleus are approximately the same.

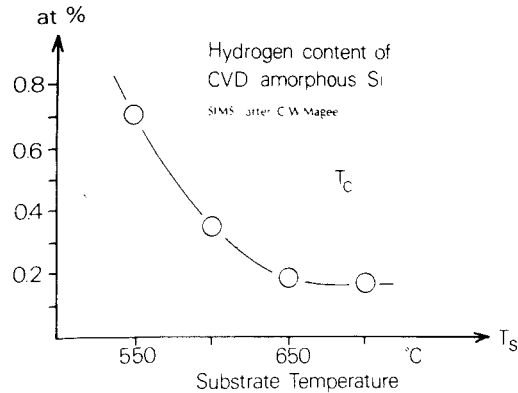


Fig. 1. Hydrogen content of non-intentionally doped CVD amorphous silicon films, determined by secondary ion mass spectroscopy [20].

For the material heavily doped with foreign atoms, the X-ray diffraction spectra, as well as transmission electron micrographs, indicate that the already crystallized areas contain a smaller concentration of dopant atoms than the remaining areas outside. The crystallization is apparently accompanied by a rejection of the dopant into the still amorphous matrix. It follows that the amorphous fraction of the volume is progressively enriched with the dopant as crystallization proceeds. One is reminded of the purification of a growing crystal in the floating zone process, although the limited diffusivity in the solid phase limits the analogy.

It follows that the rate of crystallization is further retarded the greater the already crystallized fraction. This is suggested by fig. 2, where the intensity of the {111} X-ray diffraction peak is plotted as a function of the length of anneal, relative to that of a standard CVD polycrystalline film. The non-intentionally doped film annealed at 650°C starts to crystallize after less than 2 h, in agreement with the results of

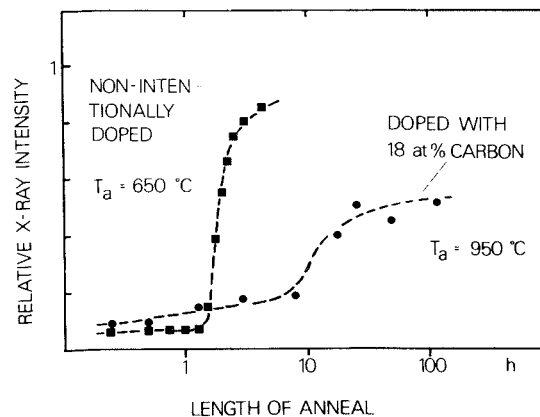


Fig. 2. Intensity of the Si{111} diffraction peak (normalized to the peak heights observed for a standard CVD polycrystalline sample) vs. annealing time, T_a .

Janai et al. [15]. In contrast, a film doped with 18 at% C withstands an anneal at 950°C for up to 10 h before substantial crystallization starts. The anneal profile, not only of the X-ray peak heights, but of the optical properties, as well, is quite different in doped films. Note, for instance, that the {111} peak in the non-intentionally doped material does not appear during an initial induction period. In carbon-doped films it grows with a finite slope right from the beginning of the anneal. The overall change is much slower, however, in spite of the much higher temperature, and results in an effective retardation of the crystallization.

Even after longtime anneal, the heights of the {111} diffraction peak fall short of the response eventually observed in crystallized non-intentionally doped material. In the doped film the crystallization apparently leaves a certain fraction of the volume amorphous, due to the residual high concentration of the dopant. Further growth of the crystalline regions subsequently proceeds at such a slow rate that it effectively ceases before all of the doped silicon is crystallized.

In order to describe the crystallization process in quantitative terms, we assigned a "crystallization time" to the occurrence of the inflection point in the profiles of fig. 2. Such a point was observed for all the dopants studied in sufficient detail. Table 2

Table 2
Crystallization time

Dopant	Concentration (at%)	Anneal temperature (°C)	Crystallization time* (h)
C	18	950	14 ± 4
C	18	990	> 2
C	18	1040	0.4 ± 0.1
C	11	1040	0.3 ± 0.1
C	18	1040	0.4 ± 0.1
C	27	1040	≈ 10
C	35	1040	> 10
N	17	950	> 90
N	17	990	> 2
N	17	1040	2 ± 1
B	< 0.5	730	< 0.25

*See text for definition. Times for 18 at% C samples are the data base for fig. 3.

summarizes the crystallization time for some dopants and anneal temperatures investigated. Plotted as a function of reciprocal absolute temperature, the logarithms of the crystallization times given in table 2 fall on a straight line. This suggests expressing the rate of crystallization in terms of an Arrhenius equation. Slope and intercept with $1/T=0$, of the profiles plotted in fig. 3 determine in this equation the activation energy and the pre-exponential factor, respectively. For non-intentionally doped silicon we obtain 78 kcal/mol (3.4 eV/atom) [24], while the material doped with 18 at% C gives (110 ± 20) kcal/mol $[(4.8 \pm 1)$ eV/atom]. Note that these activation

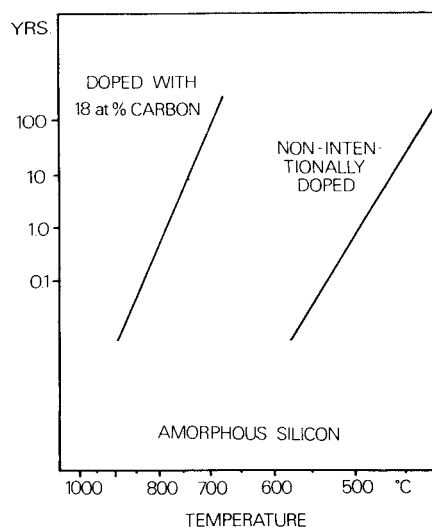


Fig. 3. Crystallization time vs. anneal temperature for CVD amorphous silicon, based on the data of table 2 for 18 at% C.

energies are roughly twice the bond energies of the Si–Si bond (42 kcal/mol) and the Si–C bond (69 kcal/mol) [25].

The straight line on the left of fig. 3 represents the most conservative assessment of the data. The straight line on the right is based on the data reported by Janai et al. [15]. Note, however, that in Janai's interpretation, a slightly different definition of the crystallization time was used, resulting in longer times for equivalent crystallization at a given temperature. While carbon and nitrogen retard the crystallization, boron does not. Note further that for a given temperature of anneal the retardation is most effective for a high concentration of the dopant. For a given carbon concentration, crystallization proceeds faster at higher temperatures of anneal, as one would expect.

From the data of fig. 3 we can draw a conclusion of technological significance for the structural lifetime of a photothermal converter surface that uses carbon-stabilized silicon as the absorber. We can determine this time span from fig. 3 to be on the order of several decades, if the surface is continuously operated at 700°C. Day–night cycles and cloudy periods extend this time interval even further. Operation at 650°C extends the crystallization time to several hundred years. If this extrapolation on the basis of the Arrhenius equation has any merit, it is apparent that the retardation of the crystallization by carbon doping contributes significantly to the structural lifetime of an amorphous silicon solar absorber.

4.2. Effects of doping on the optical properties

Retarding the crystallization becomes particularly valuable if the dopants stabilizing the amorphous phase change, at the same time, the optical properties in the direction of an increased solar absorptance. We describe in this section first the effect of the

doping on the absorption coefficient of the film, then on its index of refraction, and finally the effect of a post-deposition anneal on both optical quantities. A paragraph on the electron spin resonance in doped films concludes the presentation of experimental results and their discussion.

4.2.1. Effects on the absorption coefficient

Fig. 4 compares the absorption coefficient of non-intentionally doped amorphous silicon films after Janai et al. [15] with that of films doped with boron, nitrogen, carbon or germanium. Note that all four dopants generate a low-energy tail in front of the absorption edge of the non-intentionally doped material. However, only in the case of carbon and boron dopants does this tail result in an increased solar absorptance, because the corresponding absorption profiles lie, respectively, above or are equal to that of the non-intentionally doped material for a sufficient width of the solar spectrum. For films doped with nitrogen or germanium, the reduction of the absorption coefficient for photon energies greater than 1.6 eV probably more than eliminates any gain in solar absorptance provided by the low-energy tail.

Fig. 5 plots the absorption coefficient of films doped with carbon at various levels of concentration. Note that the gain in solar absorptance is most pronounced for films doped with 18 at% C. In films doped with a higher concentration, the profile of the absorption coefficient drops below that of the non-intentionally doped material above photon energies of 1.6 eV.

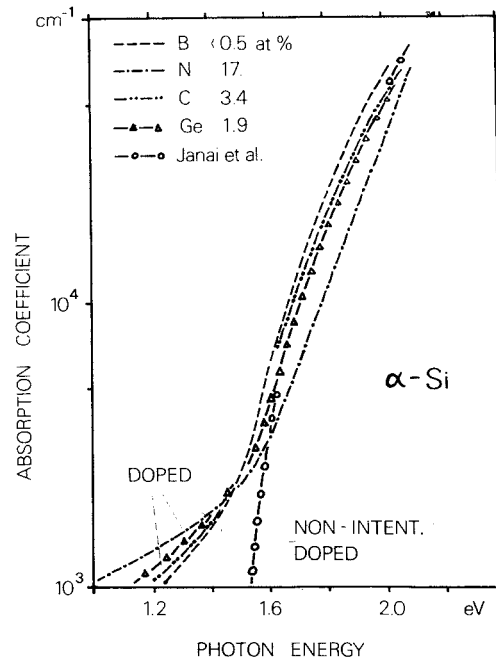


Fig. 4. Absorption coefficient as function of photon energy for CVD amorphous silicon doped with boron, nitrogen, carbon or germanium.

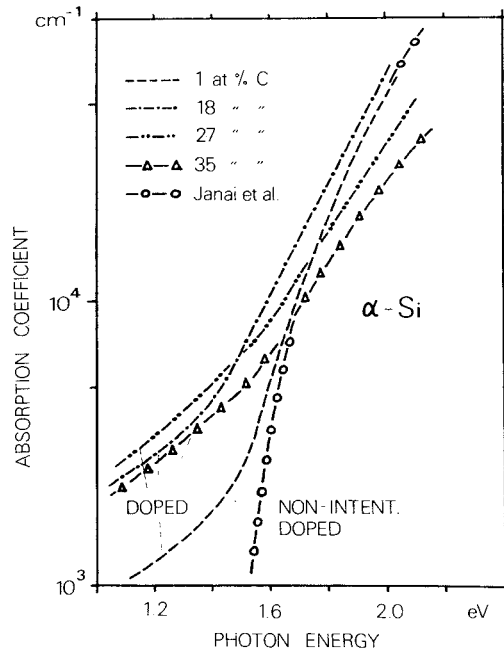


Fig. 5. Absorption coefficient as function of photon energy for CVD amorphous silicon doped with various concentrations of carbon.

A frequently used quantity for comparing the optical properties of amorphous semiconductors is the optical gap E_0 , defined by:

$$\sqrt{\alpha h\nu} = A(h\nu - E_0), \quad (2)$$

where α is the absorption coefficient, A is a constant and E_0 is the energy of the band gap. By extrapolating the straight portion of eq. (2), an approximation to the value of E_0 is obtained. We found for our doped samples values from 1.50 to 1.65 eV, compared to 1.60 eV for the non-intentionally doped amorphous silicon. Glow-discharge-produced amorphous silicon carbide films show values of 2.25 to 3.0 eV, as reported by Anderson and Spear [22].

4.2.2. Effects on the index of refraction

Fig. 6 plots the index of refraction for films doped with boron, nitrogen, carbon or germanium. The doping results in a lowering of the index of refraction as compared to the non-intentionally doped material for the three dopants that are on the same column or to the right of silicon in the periodic system. Boron – one column to the left of silicon – increases the refractive index significantly. The character of the charge transfer upon forming the Si–B bond can speculatively lead to an electron distribution that is more easily polarized than the Si–Si bond, thus increasing the index of refraction of the alloy over the elemental lattice [26]. Further work is required to support this speculation, however.

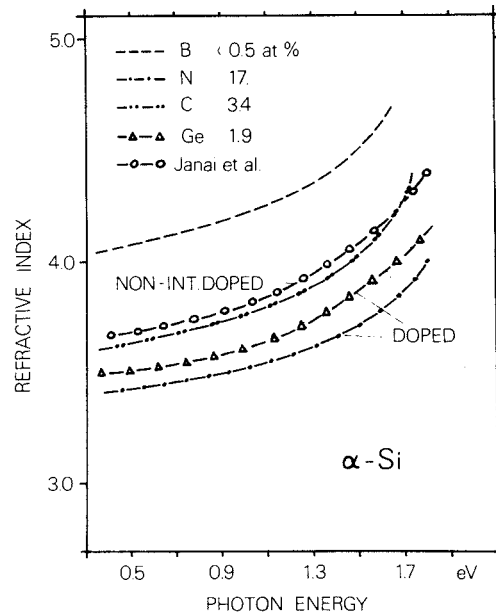


Fig. 6. Refractive index as function of photon energy for CVD amorphous silicon doped with boron, nitrogen, carbon or germanium.

The lowering of the refractive index compared to the non-intentionally doped material, is more pronounced the higher the concentration of the carbon dopant, as shown in fig. 7.

4.2.3. Effects of annealing on absorption coefficient and index of refraction

Our study of the crystallization of carbon-doped films had shown that noticeable changes could only be expected in a reasonable laboratory time frame, if an anneal proceeded close to the 1000°C temperature mark. Consequently, we measured the changes in absorption coefficient and index of refraction that accompany the crystallization after anneals of various lengths at 990°C. The results are shown in figs. 8 and 9 for a set of films doped with 18 at% carbon.

Two features are common to both absorption coefficient and refractive index. First, the optical properties respond already to the small structural changes that precede the inflection point from which the crystallization time was derived. Extrapolation of the Arrhenius plot in fig. 3 gives a crystallization time of approximately 120 min for the anneal temperature of 990°C. The optical changes plotted in figs. 8 and 9 occur within times that are shorter by one order of magnitude. This indicates that the optical properties are sensitive to the small structural changes that precede the rapid rise towards the inflection point.

Note secondly that no further changes are observed after an anneal of 120 min at 990°C. Neither absorption coefficient nor index of refraction show further changes if the anneal is extended beyond this time.

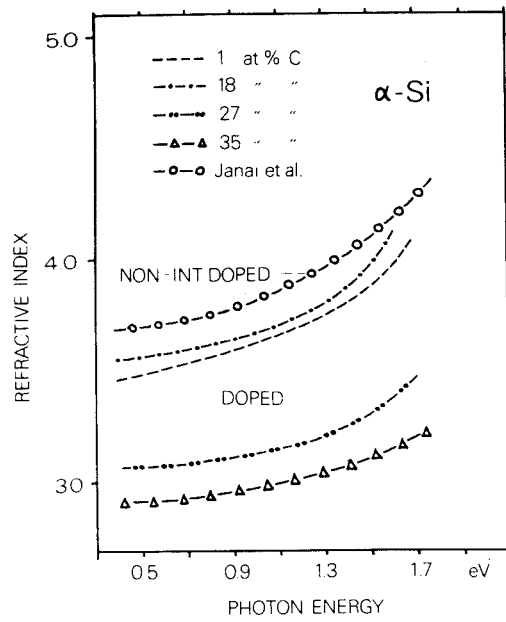


Fig. 7. Refractive index as function of photon energy for CVD amorphous silicon doped with various concentrations of carbon.

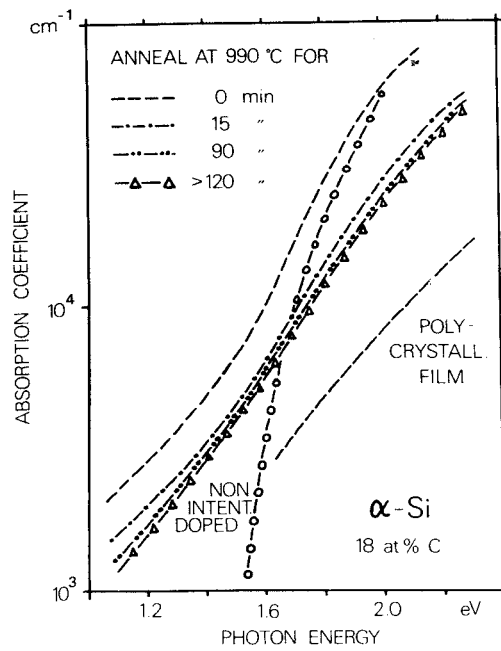


Fig. 8. Absorption coefficient as function of time for CVD amorphous silicon films doped with 18 at% C after anneal at 990°C for various lengths of time.

The spectral profile of the absorption coefficient is shifted towards higher photon energies as the anneal proceeds. This reduces the solar absorptance. Note, however, that the spectral shift upon crystallization is arrested long before the spectral profile of a crystallized non-intentionally doped amorphous sample is reached, marked "polycrystalline film" in fig. 8. This implies that the doped film has a solar absorptance superior to that of the non-intentionally doped absorber, even if both films have been exposed to anneals at extremely high temperatures. This further supports the assumption that the crystallization in the doped samples proceeds in a manner different from that of the non-intentionally doped material and probably does not run to completion.

Fig. 9 shows that the refractive index, too, is shifted towards larger photon energies without much change in the shape of the spectral profile. The shift comes to a halt after 120 min of anneal.

4.3. Effects of doping on the electron spin resonance

Through the collaboration of P. Gaczi at the James Franck Institute of the University of Chicago [19], the electron spin resonance of a number of non-intentionally doped samples deposited at various substrate temperatures, as well as a set of samples doped with carbon at various levels of concentration, was investigated. For the non-intentionally doped samples deposited at comparable substrate temperatures, the results are largely in agreement with those of Hirose and coworkers [23]. In the

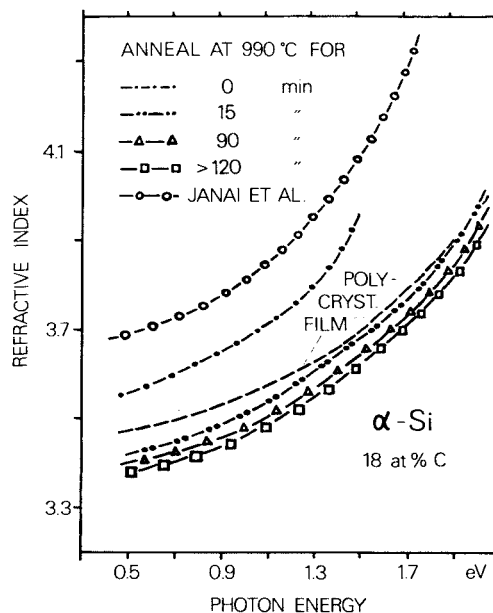


Fig. 9. Refractive index as function of time for CVD amorphous silicon doped with 18 at% C after anneal at 990°C for various lengths of time.

carbon-doped samples, the number of free spins associated with dangling bonds increased with the concentration of carbon atoms in the lattice. The additional spins are associated with silicon atoms rather than with the carbon dopant. The results are consistent with the assumption that the hydrogen incorporated into the film is bonded to the carbon rather than terminating the dangling bonds in the amorphous silicon matrix. This is to be expected from a C–H bond energy that is larger than the Si–H bond energy. The work is in progress and will be reported on in a later publication.

5. Stabilized amorphous silicon films in solar converter stacks

5.1. Solar absorbers of stabilized amorphous, non-intentionally doped amorphous, and polycrystalline silicon – a comparison

To assess the relative merits of materials in terms of their solar absorptance based on the differences in the spectral profile of their absorption coefficients is not a straightforward method. Since the solar absorptance a is given by

$$a = \int_0^{\infty} \alpha_h(\lambda) \Phi_s(\lambda) d\lambda / \int_0^{\infty} \Phi_s(\lambda) d\lambda, \quad (3)$$

the value of the hemispherical spectral absorptance $\alpha_h(\lambda)$ must be multiplied by the solar flux $\Phi_s(\lambda)$ and normalized to the entire solar output. This is conveniently done by plotting the optical properties – reflectance or absorptance – of the converter surface on a “distorted λ -plot” that is linear in fractions of the solar spectrum. The solar absorptance is derived from such a plot by simple planimetry of the areas cut out by either reflectance or absorptance spectrum with the area of the entire graph representing 100% [27].

We show in fig. 10 the absorptance profile derived from

$$A(\lambda) = 1 - \exp[-2\alpha(\lambda)d] \quad (4)$$

for polycrystalline, non-intentionally doped amorphous and stabilized amorphous silicon (18 at% C) films for a thickness of 1 μm films. To interpret the areas above the curves in terms of solar absorptance, the reflection loss at the absorber/air interface must be taken into account.

Note first that the profile for the non-intentionally doped amorphous silicon film is much steeper than that for the polycrystalline film. This implies that amorphous silicon is superior to the polycrystalline material, in particular for thin films, since a steep edge moves much less with thickness than a shallow one. Thus it follows that a given absorptance value can be obtained from an amorphous film that is much thinner than the absorptance-equivalent polycrystalline film. We wish to stress this point with respect to design and performance of the entire reflector–absorber stack. The interference fringes generated from multiple reflections at the top and bottom surfaces of the absorber layer are, in their spectral position, of importance for the performance of the stack. With a much smaller thickness of the amorphous silicon

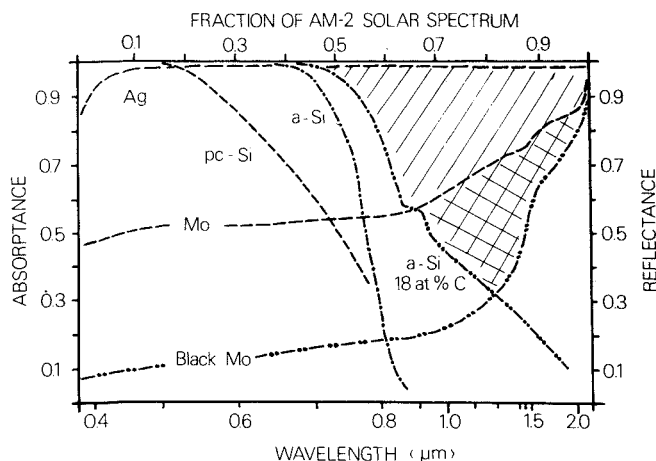


Fig. 10. Double-pass absorptance through a $1 \mu\text{m}$ thick sample of polycrystalline silicon (pc-Si) [15], non-intentionally doped amorphous silicon (a-Si) [15], and stabilized amorphous silicon (a-Si, 18 at% C) plotted on a distorted λ -plot. Superimposed are the reflectances of silver, CVD molybdenum [29] and black molybdenum [31]. Shaded and crosshatched areas qualitatively correspond to the gain in absorptance over a silver reflector. Note that kinks in the curves are caused by irregularities of the distorted λ -plot that represent absorption bands in the solar spectrum.

absorber, the first fringe is located in a part of the spectrum where it degrades the performance least [28].

We note for the stabilized amorphous silicon film of fig. 10 that while the absorption edge is no longer as steep as that of the non-intentionally doped material, it is now slanted to longer wavelengths due to the long wavelength tail of the absorption coefficient. This absorption tail adds to the solar absorptance of a stack based on the stabilized material.

5.2. Stabilized amorphous silicon in absorber-reflector tandems

Besides its thickness, the proper match of the optical spectrum of the absorber layer to that of the reflector beneath is of importance for the performance of the entire stack. For this reason, we have plotted the reflectance spectra of three reflector materials – silver, highly reflecting molybdenum [29], and black molybdenum [30] – on the distorted λ -diagram of fig. 10. The high reflectance of silver in the infrared rejects solar photons that pass through the absorber beyond its absorption edge. Molybdenum performs much better in this respect, since it reaches its high infrared reflectance of more than 97.4% only beyond the extension of the solar spectrum at the right hand side of fig. 10 [29].

The optimal match to the absorption profile of amorphous silicon is given by the reflectance profile of black molybdenum, a CVD film prepared by the pyrolytic decomposition of molybdenum carbonyl in the presence of oxygen [30]. With an anti-reflection coating of Si_3N_4 , such stacks are reported to absorb up to 91% of the incident solar flux [31]. By adding an optimal thickness of stabilized absorber between

the Si_3N_4 layer and the black molybdenum reflector, it is potentially possible to improve on this value. It is important in this context that the optical constants of silicon provide a much better match to those of molybdenum than other dielectrics customarily used for anti-reflection layers [28].

We are presently engaged in the fabrication, testing and evaluation of photothermal converter stacks based on molybdenum reflectors and stabilized or non-intentionally doped amorphous silicon absorbers. It has been shown feasible to deposit silicon directly on molybdenum with no destructive effects to the molybdenum, and such stacks with an anti-reflection coating of Si_3N_4 have withstood 500 h testing in air at 500°C without apparent interdiffusion of the layers or degradation of the molybdenum reflector. In addition, stacks consisting of 1000 \AA of carbon stabilized amorphous silicon on molybdenum without the protection of an anti-reflection layer have withstood 750 h at 500°C in air with little or no reduction of the infrared reflectance [32, 33]. Future work will be concerned with optimizing the thicknesses of the absorber and anti-reflection layers to produce a maximum solar absorptance and will be reported on at a later time.

References

- [1] H. Tabor, *Trans. Conf. Use Solar Energy* 2, 1A (1955) p. 32; *Bull. Res. Council Israel* 54 (1956) p. 28.
- [2] J. T. Gier and R. V. Dunkle, *Trans. Conf. Use Solar Energy* 2, 1A (1955) p. 41.
- [3] D. M. Mattox, *J. Vac. Sci. Technol.* 13 (1976) 127.
- [4] B. O. Seraphin and A. B. Meinel, in: *Optical Properties of Solids – New Developments*, ed. B. O. Seraphin, (North-Holland, Amsterdam, 1975) ch. 17 p. 927.
- [5] R. E. Hahn and B. O. Seraphin, *J. Vac. Sci. Technol.* 12 (1975) 905.
- [6] B. O. Seraphin, in: *Solar Energy Conversions – Solid State Physics Aspects*, *Topics in Applied Physics* 31, ed. B. O. Seraphin (Springer-Verlag, Berlin–Heidelberg–New York, 1979) p. 5.
- [7] D. K. Edwards, J. T. Gier, K. E. Nelson and R. D. Roddick, *Proc. UN Conf. New Sources of Energy* (United Nations, New York, 1964) vol. 4.
- [8] V. A. Wells, B. O. Seraphin and J. S. Raymond, *Proc. 4th Intern. Conf. CVD* (Electrochemical Society, New York, 1973) p. 512.
- [9] R. E. Hahn and B. O. Seraphin, in: *Physics of Thin Films* 10, ed. G. Hass (Academic Press, New York, 1978) p. 1.
- [10] D. C. Booth, M. Janai, G. Weiser, D. D. Allred and B. O. Seraphin, *Proc. Soc. Photo-Optical Instr. Eng. (SPIE)* 161/IV (1978) p. 72.
- [11] *Proc. Symp. on Material Sciences Aspects of Thin Film Systems in Solar Energy Conversion*, ed. B. O. Seraphin, Tucson, AZ (1974); NSF-RANN Grant GI-43-795, 7 (1974).
- [12] B. O. Seraphin, *J. Japan. Soc. Appl. Phys.* 44 (1975) 11.
- [13] R. W. Griffith, *Sharing the Sun – Solar Technology in the Seventies*, Winnipeg, Canada (1975) *Intern. Solar Energy Soc.* 6 (1976) 205.
- [14] M. H. Brodsky, M. A. Frisch, J. F. Ziegler and W. A. Lanford, *Appl. Phys. Lett.* 30 (1977) 561.
- [15] M. Janai, D. D. Allred, D. C. Booth and B. O. Seraphin, *Solar Energy Mater.* 1 (1979) 11.
- [16] T. I. Kamins and D. J. Delloca, *J. Electrochem. Soc.* 119 (1972) 112.
- [17] G. A. N. Connell, W. Paul and R. J. Temkin, *Adv. Phys.* 22 (1973) 643.
- [18] The authors would like to thank K. Seshan, Metallurgy Department, University of Arizona for assisting in the TEM studies.
- [19] The authors wish to thank P. Gaczi and H. Fritzsche, University of Chicago for the ESR measurements.

- [20] The authors would like to thank C. W. Magee, RCA Laboratories, Princeton, New Jersey for the SIMS measurements.
- [21] H. Fritzsche, C. C. Tsai and P. Persans, *Solid State Technol.* 21 (1978) 55.
- [22] D. A. Anderson and W. E. Spear, *Phil. Mag. A* 35 (1977) 1.
- [23] M. Hirose, M. Taniguchi and Y. Osaka, in: *Amorphous and Liquid Semiconductors*, ed. W. E. Spear (Centre for Industrial Consultancy and Liason, University of Edinburgh, 1977) p. 352.
- [24] N. A. Blum and C. Feldman, *J. Non-Crystalline Solids* 11 (1972) 242.
- [25] F. A. Cotton and G. Wilkinson, *Adv. Inorg. Chem.* 2nd ed. (Interscience, Wiley, New York, 1966) p. 100.
- [26] *Ibid.*, p. 101.
- [27] L. F. Drummeter and G. Hass, *Phys. Thin Films* 2 (1964) 305.
- [28] D. C. Booth and B. O. Seraphin, *Proc. 2nd Ann. Conf. on Absorber Surfaces for Solar Receivers*, Boulder, CO, USA (24–25 January 1979).
- [29] G. E. Carver and B. O. Seraphin, *Appl. Phys. Lett.* 34 (1979) 279.
- [30] G. E. Carver, *Solar Energy Mater.* 1 (1979) 357.
- [31] G. E. Carver, *Thin Solid Films*, to be published.
- [32] *Tech. Rept. Grant ER-78-S-02-4899*, U.S. Dept. of Energy (1979).
- [33] *Tech. Rept., Grant EY-76-S-04-3709*, U.S. Dept. of Energy (1979).